RESEARCH ARTICLE

WILEY

Spectral analysis of continuous redox data reveals geochemical dynamics near the stream-aquifer interface

Corey D. Wallace¹ Audrey H. Sawyer¹ Rebecca T. Barnes²

Correspondence

Corey D. Wallace, School of Earth Sciences, The Ohio State University, Columbus, OH 43210.

Email: wallace.845@osu.edu

Funding information

National Science Foundation, Grant/Award Numbers: EAR-1752995 and EAR-1446724

Abstract

Changes in streamflow and water table elevation influence oxidation-reduction (redox) conditions near river-aguifer interfaces, with potentially important consequences for solute fluxes and biogeochemical reaction rates. Although continuous measurements of groundwater chemistry can be arduous, in situ sensors reveal chemistry dynamics across a wide range of timescales. We monitored redox potential in an aquifer adjacent to a tidal river and used spectral and wavelet analyses to link redox responses to hydrologic perturbations within the bed and banks. Storms perturb redox potential within both the bed and banks over timescales of days to weeks. Tides drive semidiurnal oscillations in redox potential within the streambed that are absent in the banks. Wavelet analysis shows that tidal redox oscillations in the bed are greatest during late summer (wavelet magnitude of 5.62 mV) when river stage fluctuations are on the order of 70 cm and microbial activity is relatively high. Tidal redox oscillations diminish during the winter (wavelet magnitude of 2.73 mV) when river stage fluctuations are smaller (on the order of 50 cm) and microbial activity is presumably low. Although traditional geochemical observations are often limited to summer baseflow conditions, in situ redox sensing provides continuous, highresolution chemical characterization of the subsurface, revealing transport and reaction processes across spatial and temporal scales in aquifers.

KEYWORDS

hyporheic, redox, riparian, spectral analysis, surface water-groundwater interactions, tidal

1 | INTRODUCTION

Riparian aquifers are dynamic settings where surface water and groundwater mix. Along converging hydrologic flowpaths, the delivery of limiting reagents enhances microbial activity and reaction rates (Bernhardt et al., 2017; McClain et al., 2003). Surface watergroundwater mixing in the bed and banks can attenuate excess nutrients and has important implications for water quality. In the banks, water table fluctuations due to storms and snowmelt mobilize labile dissolved organic carbon (DOC), which stimulates microbial activity and nutrient removal from surface water and groundwater (Harms & Grimm, 2008). These effects are likely magnified in tidal rivers, which have large, daily fluctuations in stage and water table elevation. Observations of dynamic reaction rates and chemical fluxes are

becoming more common (MacDonald, Levison, & Parker, 2017; Opsahl, Musgrove, & Slattery, 2017) but remain relatively scarce due to the difficulty of collecting groundwater samples with high temporal or spatial resolution during extreme events such as storms.

Alternatively, oxidation–reduction potential (E_h) can be continuously monitored using in situ sensors. E_h indicates the energetic favourability of a given reaction and has been used to describe the potential for degradation of anthropogenic contaminants in aquifers (McMahon & Chapelle, 2008). In riparian aquifers and wetlands, several factors affect the supply of reactants and rate of processing, including sediment lithology, hydrologic variability, and temperature. These drivers can interact and tend to alternately dominate in different settings. Vorenhout, van der Geest, van Harum, Wattel, and Eijsackers (2004) illustrated how lithology controlled the magnitude

¹School of Earth Sciences, The Ohio State University, Columbus, Ohio

² Environmental Studies Program, Colorado College, Colorado Springs, Colorado

of redox response to tides, whereas in other settings, E_h gradients were surprisingly stable due to the lithology (Sawyer, Kaplan, Lazareva, & Michael, 2014). Other studies suggest hydrologic variability as the dominant factor, as it is often a direct control of oxygen transport. For example, tides are a significant control on redox biogeochemistry in coastal regions (Ensign, Piehler, & Doyle, 2008), whereas permanently saturated soils tend to promote reducing conditions (e.g., Seybold, Mersie, Huang, & McNamee, 2002). Given that hydrologic forcings occur at timescales ranging from hours (Mitchell & Branfireun, 2005; RoyChowdhury et al., 2018) to months (Faulkner & Patrick, 1992; Thomas, Miao, & Sindhoj, 2009), the ability to monitor subsurface redox conditions at these timescales is critical.

In situ redox sensors generate high-resolution, continuous time series data that can be analysed in the frequency domain. Traditional spectral analysis such as the fast Fourier transform (FFT) quantifies the frequency content of a signal; wavelet analysis can be used to determine how the frequency content changes over time. These methods have been used with a variety of hydrologic sensors to study watershed processes such as rainfall and run-off (Pandey, Lovejoy, & Schertzer, 1998) over a range of timescales from years (climate and land use change) to seconds (turbulence; Thompson & Katul, 2012). For example, Henderson, Day-Lewis, and Harvey (2009) used spectral and wavelet analyses of temperature data to identify the location and timing of submarine groundwater discharge. Application of these techniques to continuous redox data can identify hydrologic drivers of geochemical transformations within riparian aquifers based on characteristic signal periods.

Spectral and wavelet analyses are potentially powerful tools in tidal rivers, which are highly dynamic environments. The riparian aquifers of tidal rivers have the potential to reduce nutrient export to the coast through denitrification and other transformations. Though their capacity to remove redox-sensitive pollutants has been recognized (Ensign et al., 2008; Ensign, Noe, & Hupp, 2014; Knights, Sawyer, Barnes, Musial, & Bray, 2017; Musial, Sawyer, Barnes, Bray, & Knights, 2016), few studies have quantified the link between tidal hydrodynamics and redox conditions. Furthermore, to our knowledge, no

study has used spectral analysis of a continuous geochemical signal to evaluate hydrologic forcings across multiple timescales. Our objective was to assess the influence of multifrequency fluctuations in river stage and water table elevation on redox conditions within the streambed and bank adjacent to a tidal river. We anticipated that redox conditions would vary semidiurnally in the banks due to tidal fluctuations in water table elevation and soil moisture. Instead, we show that tidal influence on geochemical conditions is largely confined to the permeable streambed, whereas storms drive large perturbations in both the bed and banks.

2 | METHODS

The study site (39.701196°N, 75.649906°W) is located approximately 17 km from the Delaware Bay in the tidal freshwater zone of White Clay Creek (Delaware, USA), a fifth-order river within the Christina River Basin. Tidal stage fluctuations of approximately 1 m occur twice daily and are fully confined to the channel. The floodplain is not tidally inundated. Though storm events can raise river stage by more than a meter, the floodplain is elevated ~2 m above the river, and therefore, overbank flow occurs rarely and did not occur during the monitoring period. Water table fluctuations extend from the channel ~30 m into the riparian aquifer (Musial et al., 2016). The streambed and bank are composed primarily of alluvial, interbedded sands, and silts (Figure 1).

A transect of piezometers and sampling ports was installed in 2014 to span part of the streambed and the zone of water table fluctuations in the bank (Figure 1). Beginning in May of 2016, water level and temperature were monitored every 15 min using nonvented shallow water-level data loggers (In-Situ TROLL 100) in the stream and one bank piezometer located approximately 5 m from the channel. Redox probes were installed in the streambed near Locations C (on sand bar), E (~6 m from stream), and G (~14 m from stream), as described in Musial et al. (2016), to capture a range of water table fluctuations (Figure 1). Each probe consisted of a fibreglass-epoxy tube

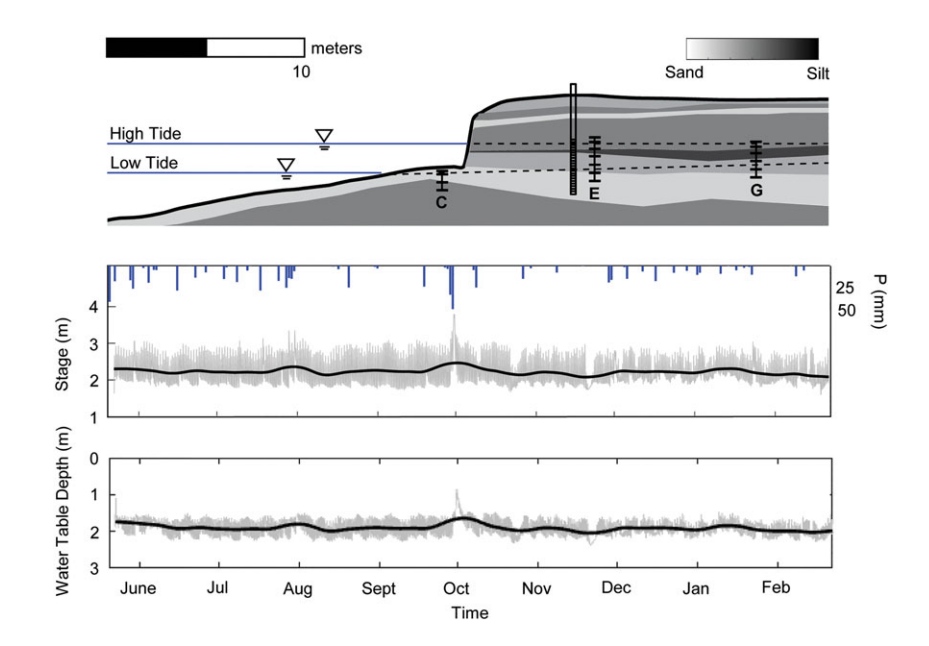


FIGURE 1 (a) Cross section showing lithology and water table positions at high and low tide. (b) Stage time series with inverted hyetograph. (c) Water table elevation time series. Redox probes are located in the streambed (Location C of Musial et al., 2016) and bank (~65 cm east of Location E and ~550 cm west of Location G of Musial et al., 2016). The piezometer contained the reference electrode. The grey lines on the time series show the unfiltered signal. Thick black lines have been filtered to remove tides

embedded with an array of 4–6 platinum electrodes spaced 15–25 cm apart (Paleo Terra, Amsterdam, Netherlands). All probes were connected to a Ag/AgCl reference electrode installed in a piezometer below the water table. To minimize agitation of the soil layer, probes were inserted directly into the undisturbed sediment. At bank Locations E and G, we augered to a depth of 130 and 135 cm, respectively, then manually inserted the probes an additional 120 and 95 cm (the respective length of each probe) into undisturbed sediments and backfilled with soil. All electrodes were connected to a CR800 control module and AM416 multiplexer (Campbell Scientific, Logan, UT) and programmed to measure every 15 min. $E_{\rm h}$ (expressed in millivolts and corrected for the potential of the standard hydrogen electrode) was logged continuously from May 2016 to February 2017. Potentials have not been corrected for pH.

On May 16, 2016, pore water samples were collected over one tidal cycle at Locations C and E (Figure 1). Surface water samples were collected on May 19, 2016. Samples were filtered to 0.45 μ m, immediately placed in a cooler, and frozen within 12 hr. Concentrations of major anions and cations were measured on Dionex ICS-5000 IC (Ion Chromatograph) and Inductively Coupled Plasma - Optical Emission Spectrometer (ICP-OES) (Table S1). Dissolved oxygen (DO) was measured at the same locations a week prior to chemical pore water measurements (May 8, 2015, and May 9, 2016) using an YSI multiparameter sonde and flow-through chamber. Given volumetric constraints, DO and ion measurements were not measured on the same samples.

The traditional FFT characterizes the general frequency content of time series data but does not characterize temporal variation in the frequency characteristics. The FFT therefore cannot resolve signal response to episodic storms or variations in tidal energy over seasons. In comparison, the continuous wavelet transformation (CWT) resolves temporal variations in energy at a given frequency, which can then be related to hydrologic events. We analysed our redox data using both the FFT and CWT. For the CWT, we used the Morlet wavelet, which is appropriate for feature extraction because it is well localized in space and time (Farge, 1992; Grinsted, Moore, & Jevrejeva, 2004):

$$\psi_0(\eta) = \pi^{-1/4} e^{i\omega_0 \eta} e^{-\eta^2/2}. \tag{1}$$

 ω_0 is dimensionless frequency (with ω_0 = 6), and η is dimensionless time. For a time series $X_{n'}$ with uniform time steps (δt), the CWT of the signal is

FIGURE 2 Comparison of raw redox time series (left) and redox contour plot (right) for Location C in the streambed. Depth-time contour plots reveal vertical redox gradients that are not readily apparent in traditional time series. Black dashed lines on the depth-time contour plot show sensor location, and river stage is shown above the depth-time contour plot for comparison

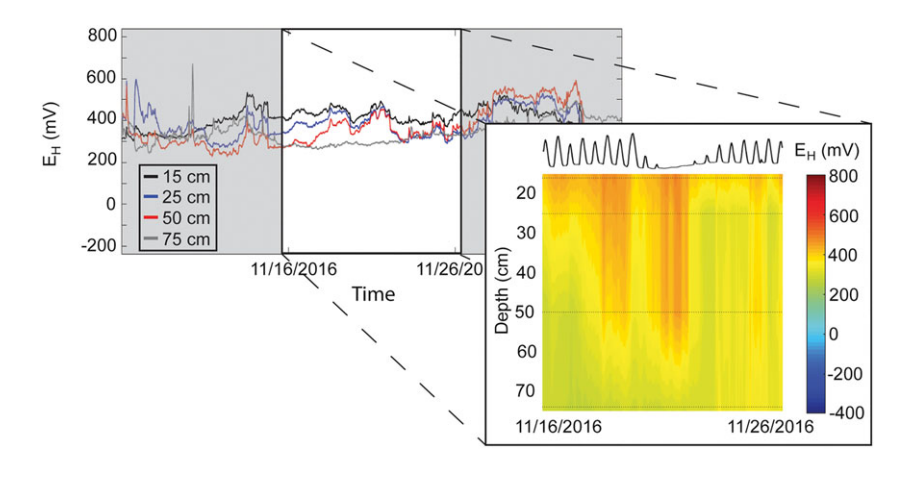
$$W_{n}^{X}(s) = \sqrt{\frac{\delta t}{s}} \sum_{n'=1}^{N} X_{n'} \psi_{0} \left[\left(n' - n \right) \frac{\delta t}{s} \right], \tag{2}$$

where s is the scale of the transformed time series $W_n^X(s)$, n is time, and n' is reversed time. The power spectrum of the CWT is represented by $|W_n^X(s)|^2$. Errors occur at the beginning and end of the wavelet power spectrum because of edge effects (shaded regions in CWT images). Wavelet analysis shows when particular frequencies in a time series are stronger or weaker, making it a powerful tool for resolving the effects of hydrologic forcings across temporal scales. For example, if a tidal frequency (0.5 days) is stronger in summer than in winter, the CWT shows higher power at that frequency during summer months.

3 | RESULTS AND INTERPRETATION

3.1 | Redox potential and geochemistry

Redox conditions differed considerably with depth (Figure 2) and between locations (Figure 3). The raw time series datasets are rich in information (Figure 2) but mask important statistics such as the median and variance of E_h at each depth, which are readily apparent in cumulative frequency distributions (Figure 3). The range of E_h values measured in the bed was generally small. Median Eh ranged from only 435 to 581 mV over 75-cm depth (Figure 3, Location C), corresponding to a vertical redox gradient of 1.95 mV/cm. All streambed depths tended to be anaerobic (E_h < 800 mV) for the majority (>99%) of the study period. Despite significant tidal exchange between surface water and the bed, oxic conditions typically extended less than 15 cm into the sediment where the shallowest electrode was located, consistent with reactive transport models (Knights et al., 2017). Nitrate (NO₃⁻) concentrations in the streambed ranged from 0.19 to 0.51 mg N/L over 75-cm depth and were low relative to NO₃⁻ concentrations in either surface water (2.69 mg NO₃⁻ N/L) or deeper groundwater, consistent with possible denitrification. Total iron (Fe; 1.6 to 2.9 mg/L) and manganese (Mn; 0.5 to 2.1 mg/L) were elevated relative to deeper groundwater (0.08 and 0.03 mg/L, respectively). Given that samples were filtered and Fe (II) is more soluble, elevated total Fe and Mn



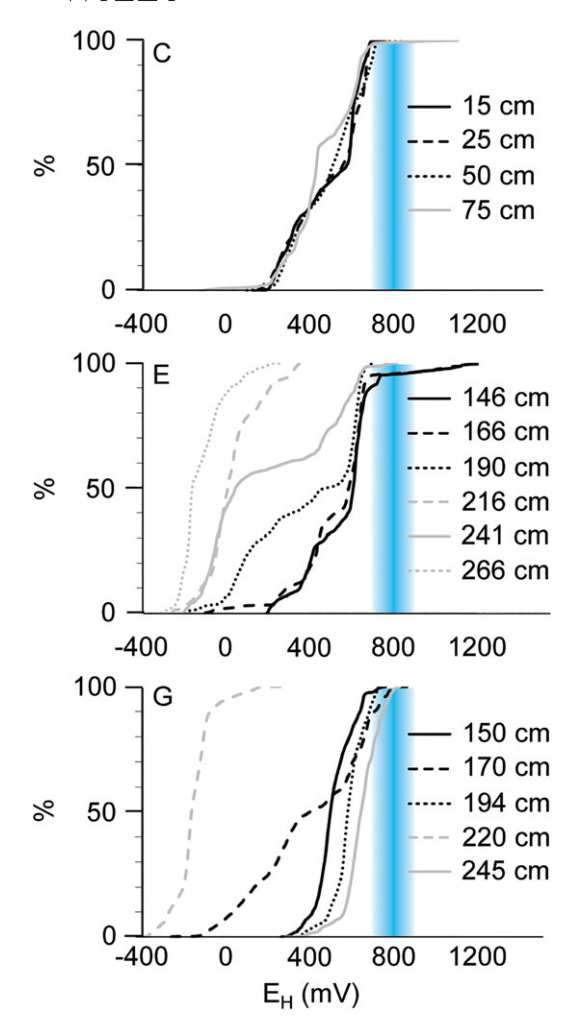


FIGURE 3 Cumulative distribution function of the redox potential at Locations C, E, and G. The blue shading indicates the transition zone between aerobic and anaerobic conditions over the range of temperatures recorded in the piezometer during the monitoring period. Water table elevation ranged from approximately 85 to 236 cm at Location E

concentrations are likely indicators of reducing conditions (Stumm & Morgan, 1996).

Within the bank (Figure 3, Locations E and G), Eh was consistently lower at depth and increased to >600 mV at the water table boundary. The vertical redox gradient, as determined from median values, was significantly greater in the banks than the bed and increased with distance from the stream. Vertical gradients were 6.4 and 8.5 mV/cm at Locations E and G, respectively; smaller water table fluctuations farther from the stream may explain the steeper vertical gradients (Musial et al., 2016). Anaerobic conditions persisted for more than 95% of the study period at Location E, where the upper two electrodes (depths 146 and 166 cm) were above the water table occasionally but likely within the capillary fringe for about 99% of the study period. Water table fluctuations likely enhanced oxygen transport, producing sporadic aerobic conditions (0.84 to 1.32 mg/L) during the sampling days in May, and presumably throughout the rest of the monitoring period. Nitrate concentrations at Location E ranged from 10.27 to 0.02 mg N/L between 220 and 300 cm, suggesting net denitrification with depth.

3.2 | Temporal dynamics

Strong seasonal changes in E_h occurred in both the bed and banks over the monitoring period. In the banks, vertical redox gradients became smaller from summer to winter (Figure 4b-d). In the bed, vertical redox gradients reversed: Eh decreased with depth in summer (Figure 4a) but increased with depth in winter (Figure 4c), when deeper sediment became slightly more oxic (increase of 200 mV) and shallower sediment became significantly more reducing (decrease of 400 mV). Seasonal temperature variation likely changes kinetic reaction rates that drive redox conditions (microbial respiration) and could contribute to the reversal. Leaf-off at the site typically occurs in midto late October, and coincident changes in the availability of labile DOC in the streambed could drive accelerated NO₃⁻ consumption and a shift towards more reducing conditions in shallow sediments (Zarnetske, Haggerty, Wondzell, & Baker, 2011; Goodale, Aber, Vitousek, & McDowell, 2005). Deeper oxidizing conditions in the streambed could potentially be explained by lateral transport of nutrients through high-permeability sediment layers. Shifts in temperature (average surface water temperature ranged from about 25°C in the summer to 5°C in the winter) cannot account for the Eh fluctuation as the 20°C shift corresponds to only 4 mV of E_h. Unfortunately, we did not collect pore water samples during winter when redox gradients were inverted.

In the frequency domain (Figure 5), water level and redox time series displayed broad peaks over long frequencies (weeks to months) that represent relatively slow perturbations due to seasons and storms. At higher frequencies, the energy spectra had power law tails that have been widely observed in hydrologic datasets (Fleming, Lavenue, Aly, & Adams, 2002; Kendall & Hyndman, 2007; Thompson & Katul, 2012). For stage and water table elevation, these tails were punctuated by peaks at tidal frequencies, indicating strong tidal fluctuations (Figure 5a). These same tidal frequencies were present in redox data at most streambed locations (e.g., Figure 5b) but were absent or minimal in redox data from the bank.

Redox amplitude spectral densities (ASDs) at the 0.5-day period from streambed FFTs were larger than those in the bank (e.g., 2.66 mV at 50 cm in the bed at Location C, compared with 1.83 mV at 146 cm in the bank at Location E; Figure 5b-c). In the bed, the ASD was greatest at 50 cm near a change in lithology (Figure 5b) but was reduced at 15 cm near the sediment-water interface (not shown), where significant interaction with surface water maintained relatively oxic conditions (Knights et al., 2017). Cross wavelet analysis shows that the streambed E_h response lagged stage by 1.5 hr at 15 cm and by 3 hr at 50 cm (Figure S1). These observations are consistent with geochemical transport due to propagation of the tidal pressure wave beneath the sediment-water interface. Tidal pumping drives vertical exchange in high-permeability streambed sediments, and the phase lag of vertical flow oscillations should increase at depth. These vertical flow oscillations can transport geochemical reactants that influence redox conditions (Bianchin, Smith, & Beckie, 2010; Rocha, Ibanhez, & Leote, 2009). ASDs in the bank decreased more with depth, declining to 1.47 mV at 266 cm. This could be due to the semiconfining silt layer at ~200 cm reducing vertical transport of oxygen and other reactants over tidal timescales in the bank.

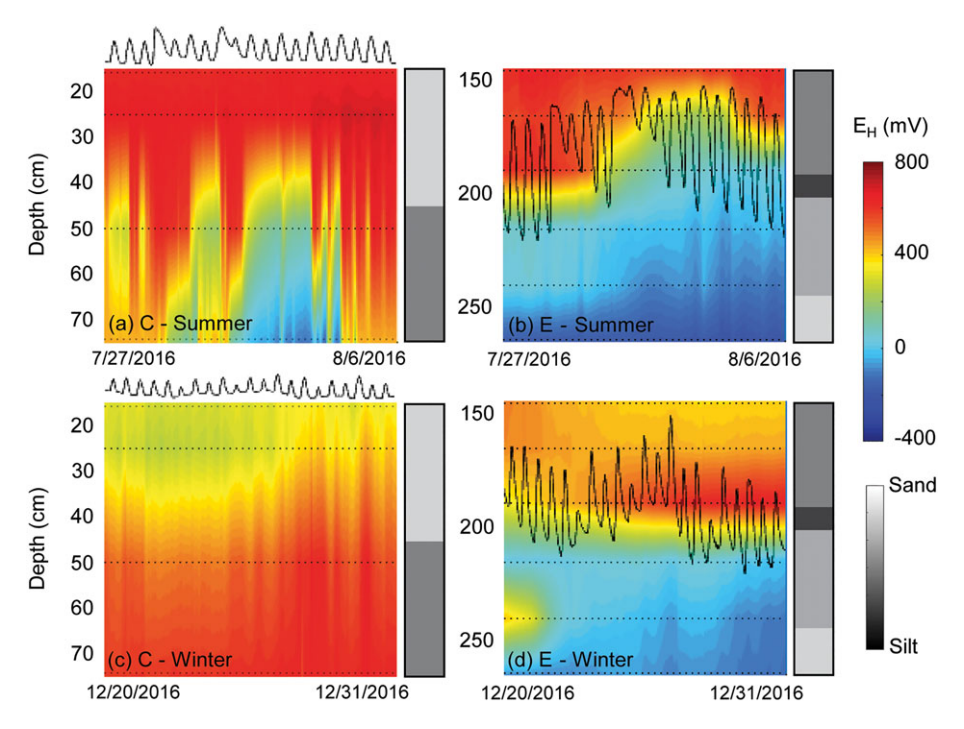


FIGURE 4 Depth-time contours of the redox signal at probe C within the streambed and probe E within the stream bank. The summer period is shown in (a) and (b), and the winter in (c) and (d). Relative river stage is indicated by the black line above (a) and (c), whereas actual water table elevation is shown on plots (b) and (d). The depth of redox electrodes are indicated by horizontal dashed lines. Aquifer lithology is shown to the right of each contour. At the beginning of the winter period, oxidizing conditions at the lowest sensor at Location E lingered from an earlier October storm

In the streambed, individual storm events drove episodic shifts towards more oxidizing conditions. On July 29 and 31, oxic conditions migrated rapidly downward, followed by recovery over hours to days (Figure 4a). Redox response to storms, like tides, increased below the shallowest sensor. During the largest storm (September 30), the response at 15 cm was moderate over periods of 4 to 8 days and was significantly greater at 75-cm depth (Figure 6). During recovery periods following storms, tidal dynamics were particularly pronounced (August 2-August 6 in Figure 4a). The strength of the tidal signal always remained subdued at 15 cm but varied over time at 50 and 75 cm (Figures 6 and 7). These variations appear to coincide with seasons and episodic storms rather than spring and neap periods. The semidiurnal E_h signal at a depth of 50 cm below the sediment-water interface was strongest in July and August (wavelet magnitude of ~5.65 mV), whereas the semidiurnal tidal signal was strongest in September and October (wavelet magnitude of ~6.69 cm; Figure 7). Wavelet magnitude of both signals was low in winter (December through February).

Redox potential in the bank responded strongly to large, episodic water table fluctuations driven by storms. During the summer, the first sizeable storm on July 29 raised the water table ~40 cm but had little effect on the redox state of the sediment profile (Figure 4). A subsequent storm on July 31 raised the water table ~50 cm and caused the anaerobic respiration front to migrate nearly 50 cm upward. As water table elevation fell, oxidizing conditions were re-established at the top of the profile over 8 days. The greatest storm responses (Figure 6) occurred in permeable layers near the water table (146 to 190 cm) and at 241 cm, where reactants could be rapidly transported (Figure 1). Storm response was minimal at 216 and 266 cm.

4 | DISCUSSION AND CONCLUSION

Continuous redox observations have great potential to reveal factors that govern aquifer geochemical conditions. Oxidizing conditions developed near the zone of water table fluctuations in the bank, reinforcing the importance of saturation in controlling subsurface redox conditions (Ensign et al., 2008; Seybold et al., 2002). Further, as the amplitude of water table fluctuations diminished away from the channel, the prevalence of aerobic conditions decreased (Locations E to G). Thus, despite the lack of strong tidal E_h oscillations near the water table (Figure 6), it appears that water table dynamics and associated saturation gradients controlled long-term average E_h in bank sediments. Lithologic variability also exerted control on prevailing patterns in E_h, with oxidizing conditions mainly observed above a semipermeable (confining) silt layer at the centre of the sediment profile (Figure 1) that likely reduced vertical transport of oxygen near the water table, resulting in a consistently steep vertical redox gradient. Similarly, in the streambed, the tidal influence on E_h was most evident at 50 cm, where coarse sand transitioned to lower permeability silty sand and a dynamic, steep redox gradient developed. The interaction of tides and sediment characteristics on redox potential was also noted by Vorenhout et al. (2004), who reported significantly dampened redox fluctuations in clay-rich, as compared to more permeable, salt marsh sediments.

In general, saturation and sediment lithology were the dominant controls on subsurface redox conditions in the banks. Increasingly steep vertical redox gradients developed from Locations E to G that were relatively stable over tidal timescales (compared with Location C in the bed). The more reducing conditions and steeper vertical gradients at G can be explained by a thinner capillary fringe and decreased solute

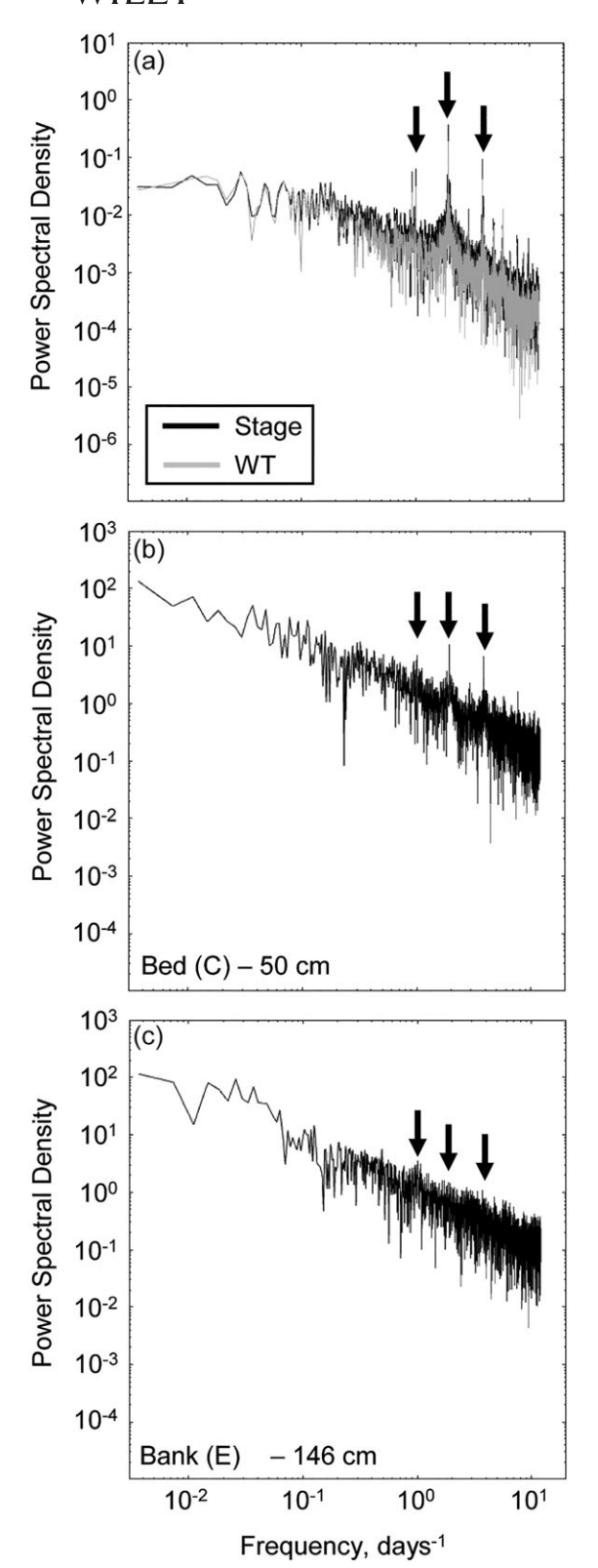


FIGURE 5 Power spectra of stage and water table elevation (a) and redox signals in the streambed (b) and stream bank (c). Peaks at the 0.25-, 0.5-, and 1-day periods are indicated by black arrows

dispersion associated with smaller water table fluctuations (Haberer, Cirpka, Rolle, & Grathwohl, 2014). The stability of E_h gradients in the banks compared with the bed can be explained not only by the greater distance to the sediment–water interface but also by the strong layering of floodplain deposits, which would impart permeability

anisotropy to the aquifer and impede vertical movement of solutes and redox gradients (Freeze & Cherry, 1979). During storm events, the prominent silty confining layer near the centre of the profile would have driven lateral flow along permeable beds in the saturated zone, allowing vertical gradients in E_h and nitrate concentrations to persist. The existence of high nitrate concentrations above this layer is consistent with potential nitrification under oxidizing conditions, whereas the nonconservative decline in nitrate concentrations below is consistent with denitrification under anaerobic conditions (Table S1). These observations collectively highlight the importance of lithology on subsurface geochemistry in the banks, similar to observations by Sawyer et al. (2014) in the nontidal portion of the same river. There, E_h in permeable gravel layers varied strongly over time during a major storm but remained moderately stable in less permeable soils.

Conversely, hydrodynamics like tidal stage fluctuations exerted an important control on subsurface redox conditions within the streambed. Vertical redox gradients were shallow compared with the banks and more dynamic over tidal timescales. Beneath the sediment-water interface, oscillatory surface water-groundwater exchange (or tidal pumping) in sandy sediments effectively transports oxygen, NO₃⁻, DOC, and other reactants (Bianchin et al., 2010; Rocha et al., 2009). Advective transport distances over individual tidal cycles were likely on the order of centimetres or less (Knights et al., 2017), but the long-term effect of oscillatory flow would enhance solute dispersion producing a shallow vertical redox gradient that fluctuates slightly over each tidal cycle. Tidal oscillations in transport were particularly evident near the lithologic boundary at 50 cm (Figure 4a). Oscillatory flow across an interface between organic and mineral sediments could control local sourcing of DOC, which often limits nitrate removal in riverbeds (Zarnetske et al., 2011). The resulting oscillations in redox gradients and presumably the denitrification front have important implications for the timing of nitrate removal and flux of nitrate to the coast in tidal rivers (Knights et al., 2017).

At all locations, long-term seasonal changes in hydrology and temperature also drive subsurface chemistry. The seasonal inversion of the redox gradient within the streambed was likely a geochemical response to changes in the amount and quality of DOC in shallow sediments. An abundance of organic matter enters the stream during autumn leaf-off, after which microbial heterotrophic activity significantly increases (Kaplan & Bott, 1983). The resulting increase in respiration rates causes a reducing shift in $E_{\rm h}$ as more energetically favourable reactants are consumed alongside DOC (Yabusaki et al., 2017).

Over seasons, the influence of tides also varied, and the use of wavelet analysis aided in detecting these changes (Figure 5). The traditional, widely used FFT is a global transform integrated over all times and is influenced by localized events regardless of when they occur (Zhou, Tang, & Chen, 2009). Although the FFT can identify whether a certain frequency component exists and can quantify its magnitude, the CWT is useful for identifying when this component appears in the record (Combes, Grossmann, & Tchamitchian, 1989). For example, a marked 0.5-day peak is seen in the FFT of the streambed E_h signal at 50 cm (ASD of 2.66 mV), but the CWT shows strong E_h response at this frequency only during the summer (wavelet magnitude of 5.62 mV; Figure 7). Interestingly, the peak in the tidal E_h response occurs in July and August, whereas the greatest tides occur in

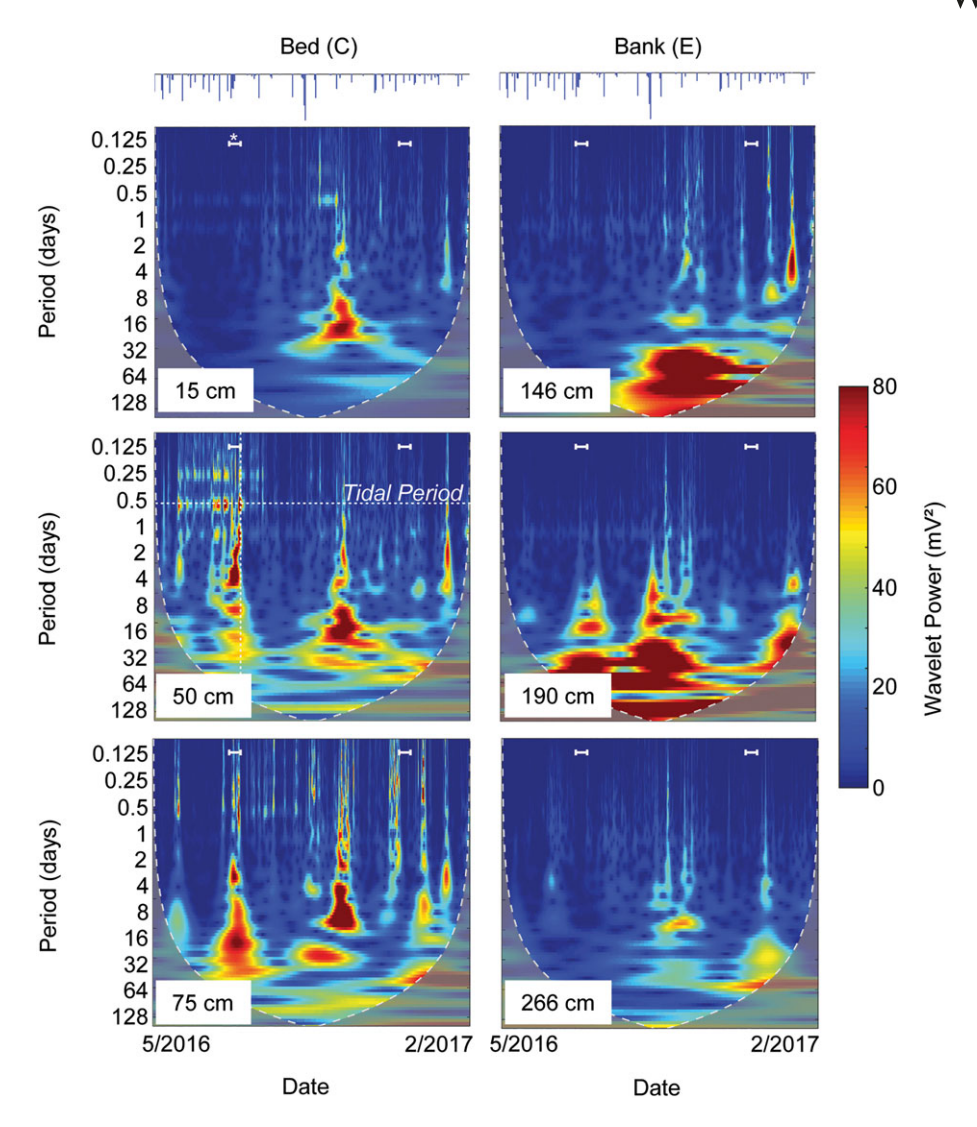


FIGURE 6 Continuous wavelet transformation of the redox signal within the streambed (left) and the stream bank (right). An inverted hyetograph above each column indicates timing of large storms. White brackets indicate the time periods displayed in Figure 3. Colours along the white horizontal dotted line indicate the power of the redox signal at the 0.5-day (tidal) period over time (also shown in Figure 7). The white vertical dotted line indicates the frequency content of the redox signal at a particular time, analogous to a Fourier transform (Figure 5b) but localized in time

September and October. Tides are expected to be large in late summer and early fall because river discharge is low, which could alter redox gradients within the streambed. The power in both the river stage signal and E_h signal diminishes during the winter (wavelet magnitude of 5.36 cm and 2.73 mV, respectively; Figure 7) when both the hydrologic forcing and microbial activity are lower.

One of the most surprising observations was the dominance of anaerobic conditions near the sediment–water interface and water table, despite moderate DO concentrations (0.52 to 1.88 mg/L) measured in pore water samples (Table S1). Pore water samples would tend to come from mobile macropores that are likely to be more oxic (Singh & Kanwar, 1991). Thus, the apparent discrepancy between in situ and ex situ geochemical data could indicate that in situ sensors are measuring net redox conditions and not preferentially sampling well-connected, high-conductivity pathways (Harvey, 1993; Harvey, Chambers, & Hoelscher, 1995; Nichol, Smith, & Beckie, 2005). Sensors could indicate the presence of reducing conditions in pore-scale microsites within largely oxic zones (Briggs, Day-Lewis, Zarnetske, &

Harvey, 2015; Holmes, Jones, Fisher, & Grimm, 1996). Past studies used isotopic tracers or measureable Fe^{2+} within shallow flow paths to identify microsites of denitrification (Harvey, Bohlke, Voytek, Scott, & Tobias, 2013; Zarnetske et al., 2011); however, these approaches traditionally require extracting groundwater, which makes continuous monitoring difficult. Further, long-term pore water extraction at high frequency can alter flow patterns and geochemical gradients. As a supplement to conventional sampling methods, in situ sensing of E_h allows for high-resolution, non-invasive chemical characterization of the subsurface environment in time and space.

Discrepancies between in situ redox data and discrete DO measurements could also reflect inaccuracies associated with traditional pore water sampling. Exposure of pore water samples to atmospheric gases could make the samples appear more oxic than in situ sensor data would indicate, though we took great care to minimize sample exposure to the atmosphere. These comparisons show that a combination of in situ and ex situ collection methods is helpful for interpreting the geochemistry of bulk groundwater.

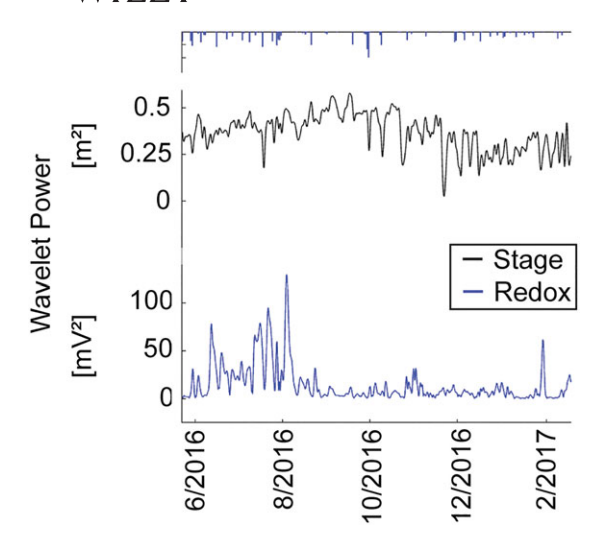


FIGURE 7 Time-series of wavelet power at the 12-hr tidal period from CWTs of redox potential 50 cm below the streambed (Figure 6) and river stage. Tidal energy in the redox signal is strongest during summer (July and August), whereas tidal energy in the river stage signal is strongest in August and September. Inverted hyetograph shows the timing of large storm events

We have shown that in situ sensing of E_h provides information about the geochemical condition of the aquifer across a broad range of timescales. Though seasonal geochemical variability can be resolved from field sampling, the effects of tides and storms are much harder to capture using traditional extraction techniques. By monitoring E_h continuously at high resolution over long time periods, the instantaneous effects of high-flow events can be resolved as effectively as long-term variability. Moreover, the regular sampling interval creates opportunities for analysis in the frequency domain. In systems where consistent sampling is difficult, or where sites become inaccessible during large storm events, the use of in situ redox sensing is advantageous for resolving spatial and temporal variability in subsurface geochemistry. By providing a continuous dataset of subsurface conditions, in situ redox measurements can be used to understand reactive transport of redox-sensitive solutes like nitrate, particularly in hydrodynamic environments such as riparian aquifers.

ACKNOWLEDGMENTS

This study was funded by the National Science Foundation (NSF EAR 1446724 and EAR 1752995). We thank Mitch Bayer for assistance in the field, Ralph and Kim Burdick for kindly providing access to the field site at the Hale Byrnes House, and Sander Smit at Paleo Terra for sensor support. Authors would also like to acknowledge Dave Montgomery, Steve Hicks, and Dave Arscott at Stroud Water Research Center for their knowledge and support. We thank Christopher Jekeli and Nlingi Habana for fruitful discussions. We also acknowledge two anonymous reviewers, whose suggestions improved this manuscript. All time series data are available on CUAHSI HydroShare website: http://www.hydroshare.org/resource/3dfee662698b4da6bc9c455bbffc35d4.

ORCID

REFERENCES

- Bernhardt, E. S., Blaszczak, J. R., Ficken, C. D., Fork, M. L., Kaiser, K. E., & Seybold, E. C. (2017). Control points in ecosystems: Moving beyond the hot spot hot moment concept. *Ecosystems*, 20, 665–682. https://doi.org/10.1007/s10021-016-0103-y
- Bianchin, M., Smith, L., & Beckie, R. (2010). Quantifying hyporheic exchange in a tidal river using temperature time series. *Water Resources Research*, 46, 1–21. https://doi.org/10.1029/2009WR008365
- Briggs, M. A., Day-Lewis, F. D., Zarnetske, J. P., & Harvey, J. W. (2015). A physical explanation for the development of redox microzones in hyporheic flow. *Geophysical Research Letters*, 42, 4402–4410. https:// doi.org/10.1002/2015GL064200
- Combes, J. M., Grossmann, A., & Tchamitchian, P. (1989). Wavelets: Time-frequency methods and phase spaceSpringer-Verlag. https://doi.org/10.1007/978-3-642-97177-8
- Ensign, S. H., Noe, G. B., & Hupp, C. R. (2014). Linking channel hydrology with riparian wetland accretion in tidal rivers. *Journal of Geophysical Research*: Earth Surface, 119, 28–44. https://doi.org/10.1002/ 2013JF002737
- Ensign, S. H., Piehler, M. F., & Doyle, M. W. (2008). Riparian zone denitrification affects nitrogen flux through a tidal freshwater river. Biogeochemistry, 91, 133–150. https://doi.org/10.1007/s10533-008-9265-9
- Farge, M. (1992). Wavelet transforms and their application to turbulence. Annual Review of Fluid Mechanics, 24, 395–457. https://doi.org/10.1146/annurev.fl.24.010192.002143
- Faulkner, S. P., & Patrick, W. H. (1992). Redox processes and diagnostic wetland soil indicators in bottomland hardwood forests. *Soil Science Society of America Journal*, *56*, 856–865. https://doi.org/10.2136/sssai1992.03615995005600030030x.
- Fleming, S. W., Lavenue, A. M., Aly, A. H., & Adams, A. (2002). Practical applications of spectral analysis to hydrologic time series. *Hydrological Processes*, 16, 565–574. https://doi.org/10.1002/hyp.523
- Freeze, R. A., & Cherry, J. A. (1979). GroundwaterPrentice-Hall.
- Goodale, C. L., Aber, J. D., Vitousek, P. M., & McDowell, W. H. (2005). Long-term decreases in stream nitrate: Successional causes unlikely; possible links to DOC? *Ecosystems*, 8, 334–337. https://doi.org/ 10.1007/s10021-003-0162-8
- Grinsted, A., Moore, J. C., & Jevrejeva, S. (2004). Application of the cross wavelet transform and wavelet coherence to geophysical time series. *Nonlinear Processes in Geophysics*, 11, 561–566. https://doi.org/10.5194/npg-11-561-2004
- Haberer, C. M., Cirpka, O. A., Rolle, M., & Grathwohl, P. (2014). Experimental sensitivity analysis of oxygen transfer in the capillary fringe. *Groundwater*, *52*, 37–49. https://doi.org/10.1111/gwat.12028
- Harms, T. K., & Grimm, N. B. (2008). Hot spots and hot moments of carbon and nitrogen dynamics in a semiarid riparian zone. *Journal of Geophysical Research*, 113, 1–14. https://doi.org/10.1029/2007JG000588
- Harvey, J. W. (1993). Measurement of variation in soil solute tracer concentration across a range of effective pore sizes. Water Resources Research, 29, 1831–1837. https://doi.org/10.1029/93WR00529
- Harvey, J. W., Bohlke, J. K., Voytek, M. A., Scott, D., & Tobias, C. R. (2013). Hyporheic zone denitrification: Controls on effective reaction depth and contribution to whole-stream mass balance. Water Resources Research, 49, 6298–6316. https://doi.org/10.1002/wrcr.20492
- Harvey, J. W., Chambers, R. M., & Hoelscher, J. R. (1995). Preferential flow and segregation of porewater solutes in wetland sediment. *Estuaries*, 18, 568–578. https://doi.org/10.2307/1352377
- Henderson, R. D., Day-Lewis, F. D., & Harvey, C. F. (2009). Investigation of aquifer-estuary interaction using wavelet analysis of fiber-optic temperature data. *Geophysical Research Letters*, 36, 1–6. https://doi.org/ 10.1029/2008GL036926.
- Holmes, R. M., Jones, J., Jeremy, B., Fisher, S. G., & Grimm, N. B. (1996).
 Denitrification in a nitrogen-limited stream ecosystem. *Biogeochemistry*, 33, 124–146. https://doi.org/10.1007/BF02181035

- Kaplan, L. A., & Bott, T. L. (1983). Microbial heterotrophic utilization of dissolved organic matter in a piedmont stream. Freshwater Biology, 13, 363–377. https://doi.org/10.1111/j.1365-2427.1983.tb00686.x
- Kendall, A. D., & Hyndman, D. W. (2007). Examining watershed processes using spectral analysis methods including the scaled-windowed fourier transform. Subsurface Hydrology, 183–200. https://doi.org/10.1029/ 171GM14
- Knights, D., Sawyer, A. H., Barnes, R. T., Musial, C. T., & Bray, S. (2017).
 Tidal controls on riverbed denitrification along a tidal freshwater zone.
 Water Resources Research, 53, 799–816. https://doi.org/10.1002/2016WR019405
- MacDonald, G., Levison, J., & Parker, B. (2017). On methods for in-well nitrate monitoring using optical sensors. *Groundwater Monitoring & Remediation*, 37, 60–70. https://doi.org/10.1111/gwmr.12248
- McClain, M. E., Boyer, E. W., Dent, C. L., Gergel, S. E., Grimm, N. B., Groffman, P. M., ... Pinay, G. (2003). Biogeochemical hot spots and hot moments at the interface of terrestrial and aquatic ecosystems. *Ecosystems*, 6, 301–312. https://doi.org/10.1007/s10021-003-0161-9
- McMahon, P. B., & Chapelle, F. H. (2008). Redox processes and water quality of selected principal aquifer systems. *Groundwater*, 46, 259–271. https://doi.org/10.1111/j.1745-6584.2007.00385.x
- Mitchell, C. P. J., & Branfireun, B. A. (2005). Hydrogeomorphic controls on reduction-oxidation conditions across boreal upland-peatland interfaces. *Ecosystems*, 8, 731–747. https://doi.org/10.1007/s10021-005-1792-9
- Musial, C. T., Sawyer, A. H., Barnes, R. T., Bray, S., & Knights, D. (2016). Surface water-groundwater exchange dynamics in a tidal freshwater zone. Hydrological Processes, 30, 739-750. https://doi.org/10.1002/hyp.10623
- Nichol, C., Smith, L., & Beckie, R. (2005). Field-scale experiments of unsaturated flow and solute transport in a heterogeneous porous medium. Water Resources Research, 41, 1–12. https://doi.org/10.1029/2004WR003035
- Opsahl, S. P., Musgrove, M., & Slattery, R. N. (2017). New insights into nitrate dynamics in a karst groundwater system gained form in situ high-frequency optical sensor measurements. *Journal of Hydrology*, 546, 179–188. https://doi.org/10.1016/j.jhydrol.2016.12.038
- Pandey, G., Lovejoy, S., & Schertzer, D. (1998). Multifractal analysis of daily river flows including extremes for basins of five to two million square kilometres, one day to 75 years. *Journal of Hydrology*, 208, 62–81. https://doi.org/10.1016/S0022-1694(98)00148-6
- Rocha, C., Ibanhez, J., & Leote, C. (2009). Benthic nitrate biogeochemistry affected by tidal modulation of Submarine Groundwater Discharge (SGD) through a sandy beach face, Ria Formosa, Southwestern India. *Marine Chemistry*, 115, 43–58. https://doi.org/10.1016/j.marchem.2009.06.003.
- RoyChowdhury, T., Bramer, L., Hoyt, D. W., Kim, Y.-M., Metz TO, McCue, L. A., ... Bailey, V. (2018). Temporal dynamics of CO₂ and CH₄ loss potentials in response to rapid hydrological shifts in tidal freshwater wetland soils. *Ecological Engineering*, 114, 104–114. https://doi.org/ 10.1016/j.ecoleng.2017.06.041
- Sawyer, A. H., Kaplan, L. A., Lazareva, O., & Michael, H. A. (2014). Hydrologic dynamics and geochemical responses within a floodplain aquifer

- and hyporheic zone during Hurricane Sandy. *Water Resources Research*, 50, 4877–1892. https://doi.org/10.1002/2013WR015101
- Seybold, C. A., Mersie, W., Huang, J., & McNamee, C. (2002). Soil redox, pH, temperature, and water-table patterns of a freshwater tidal wetland. Wetlands, 22, 149–158. https://doi.org/10.1672/0277-5212(2002)022[0149:SRPTAW]2.0.CO;2
- Singh, P., & Kanwar, R. S. (1991). Preferential solute transport through macropores in large undisturbed saturated soil columns. *Journal of Environmental Quality*, 20, 295–300. https://doi.org/10.2134/jeq1991.0047242500200010048x.
- Stumm, W., & Morgan, J. J. (1996). Redox conditions in natural waters. In Aquatic chemistry: Chemical equilibria and rates in natural waters (pp. 464-477). Wiley.
- Thomas C. R, Miao S, Sindhoj E. (2009). Environmental factors affecting temporal and spatial patterns of soil redox potential in Florida Everglades wetlands. Wetlands, 29: 1133–1145 https://doi.org/10.1672/08-234.1.
- Thompson, S. E., & Katul, G. G. (2012). Multiple mechanisms generate Lorentzian and 1/fa power spectra in daily stream-flow time series. Advances in Water Resources, 37, 94–103. https://doi.org/10.1016/j. advwatres.2011.10.010
- Vorenhout, M., van der Geest, H. G., van Harum, D., Wattel, K., & Eijsackers, H. J. P. (2004). Automated and continuous redox potential measurements in soil. *Journal of Environmental Quality*, 33, 1562–1567. https://doi.org/10.2134/jeq2004.1562
- Yabusaki, S. B., Wilkins, M. J., Fang, Y., Williams, K. H., Arora, B., Bargar, J. R., ... Wainwright, H. M. (2017). Water table dynamics and biogeochemical cycling in a shallow, variably-saturated floodplain. Environmental Science and Technology, 51, 3307–3317. https://doi.org/10.1021/acs.est.6b04873
- Zarnetske, J. P., Haggerty, R., Wondzell, S. M., & Baker, M. A. (2011). Dynamics of nitrate production and removal as a function of residence time in the hyporheic zone. *Journal of Geophysical Research*, 116, 1–12. https://doi.org/10.1029/2010JG001356
- Zhou, S., Tang, B., & Chen, R. (2009). Comparison between non-stationary signals: Fast Fourier transform and wavelet analysis. *International Asia* Symposium on Intelligent Interaction and Affective Computing, IEEE, 128–129.

SUPPORTING INFORMATION

Additional supporting information may be found online in the Supporting Information section at the end of the article.

How to cite this article: Wallace CD, Sawyer AH, Barnes RT. Spectral analysis of continuous redox data reveals geochemical dynamics near the stream-aquifer interface. *Hydrological Processes*, 2019;33:405–413. https://doi.org/10.1002/hyp.13335